Soft Matter

Accepted Manuscript

This article can be cited before page numbers have been issued, to do this please use: M. Amin Belahouane, M. Robinson, L. Grant, O. Young, G. Zorn and L. Caire da Silva, *Soft Matter*, 2026, DOI: 10.1039/D6SM00295A.

ROYAL SOCIETY OF CHEMISTRY

rsc.li/soft-matter-journal

View Article Online
DOI: 10.1039/D6SM00295A

ARTICLE

Metal-Ion Induced Coacervation of a Short Peptide under Acidic Conditions

Received 00th January 20xx,
Accepted 00th January 20xx

DOI: 10.1039/x0xx00000x

Mohammed Amin Belahouane,[a] Morgan Robinson, [a] Liam Grant, [a] Olivia Young , [a] George Zorn, [a] and Lucas Caire da Silva [a]

Coacervates formed from short peptides have recently emerged as versatile soft materials with applications in catalysis and biomimetic systems. However, liquid–liquid phase separation of short peptides typically requires charge neutralization, limiting coacervate formation under acidic conditions. Here, we show that Zn^{2+} induces coacervation of a diphenylalanine methyl ester in acidic media. This results in peptide-rich, low-polarity droplets that persist for several hours before undergoing a liquid-to-solid transition into fibrous assemblies. Spectroscopic and compositional analyses reveal that Zn^{2+} is enriched in the dense phase and interacts with peptide carbonyl groups while remaining partially hydrated. Computational calculations support this mechanism, showing that direct Zn^{2+} to carbonyl coordination is energetically unfavorable in aqueous solution, consistent with the small carbonyl shifts observed by FTIR. Despite these weak interactions, Zn^{2+} promotes coacervation under high ionic strength conditions. The addition of secondary metal ions further suppresses solidification, stabilizing coacervates for up to seven days without fiber formation. Co-metals also modulate droplet properties such as polarity and viscosity, enabling fine control over the coacervate phase. Together, these findings demonstrate that metal–peptide interactions can regulate phase behavior in minimal peptide systems at low pH and provide a strategy for designing metal-responsive coacervates.

Introduction

Liquid-liquid phase separation (LLPS) is a fundamental mechanism by which a homogenous solution spontaneously reorganizes into a dense, concentrated liquid phase (coacervates) and a coexisting dilute phase.[1-3] In biology, LLPS underlies the formation of membraneless organelles that concentrate and regulate biochemical processes, such as stress granules, P-bodies, and the nucleolus.[4-6] Coacervates have also emerged as versatile model systems and functional building blocks in soft matter engineering. Examples include the study of phase separation in aqueous media and the engineering of functional and dynamic liquid-like microenvironments to create life-like dynamic chemical systems.[7-12]

Most synthetic coacervates rely on complex electrostatic interactions between oppositely charged macromolecules.[13-16] These systems are typically water-rich (>70% by weight) and form under near-neutral conditions.[17, 18] In contrast, generating low polarity coacervates remains challenging. Minimalistic peptide systems offer a promising route to hydrophobic coacervates as their formation is driven by non-charge interactions including hydrophobic effects, π–π stacking and hydrogen bonding.[19, 20] Ultrashort peptides (2-3 amino acids) have recently been introduced as a promising class of molecules that form low-polarity, water-poor coacervates. A major advantage of ultrashort peptide-based coacervates is that their properties are highly sensitive to composition and therefore easily encoded at the molecular level.[21-25]

Ultrashort peptides typically undergo LLPS only under conditions in which their net charge is neutralized, most often via deprotonation of a N-terminal amino group. This deprotonation reduces electrostatic repulsion and promotes intermolecular association.[26-28] Under acidic conditions however, protonation increases charge repulsion and peptide solubility, suppressing phase separation. As a result, the formation of coacervates from charged ultrashort peptides under such conditions remains elusive.

Metal ions are well known to modulate self-assembly in soft materials through screening, dehydration, and coordination effects.[29-32] In macromolecular systems, multivalent ions can induce condensation or gelation, yet metal-triggered LLPS in minimal peptide systems has been scarcely explored. Understanding how metal-peptide interactions influence phase behavior, internal organization, and transformation pathways would expand the design principles of peptide-based soft materials.

Here we show that Zn^{2+} induces coacervation of a model minimal peptide, diphenylalanine methyl ester (FF-OMe), under acidic conditions (pH 3.3-4), generating hydrophobic, peptide-rich droplets that persist for hours before undergoing a liquid-solid transition into fibers. Compositional analysis,

[a] McGill University, Department of Chemistry, Montreal H3A 0B8, Canada.
Email: lucas.cairedasilva@mcgill.ca

View Article Online
DOI: 10.1039/D5SM01295A

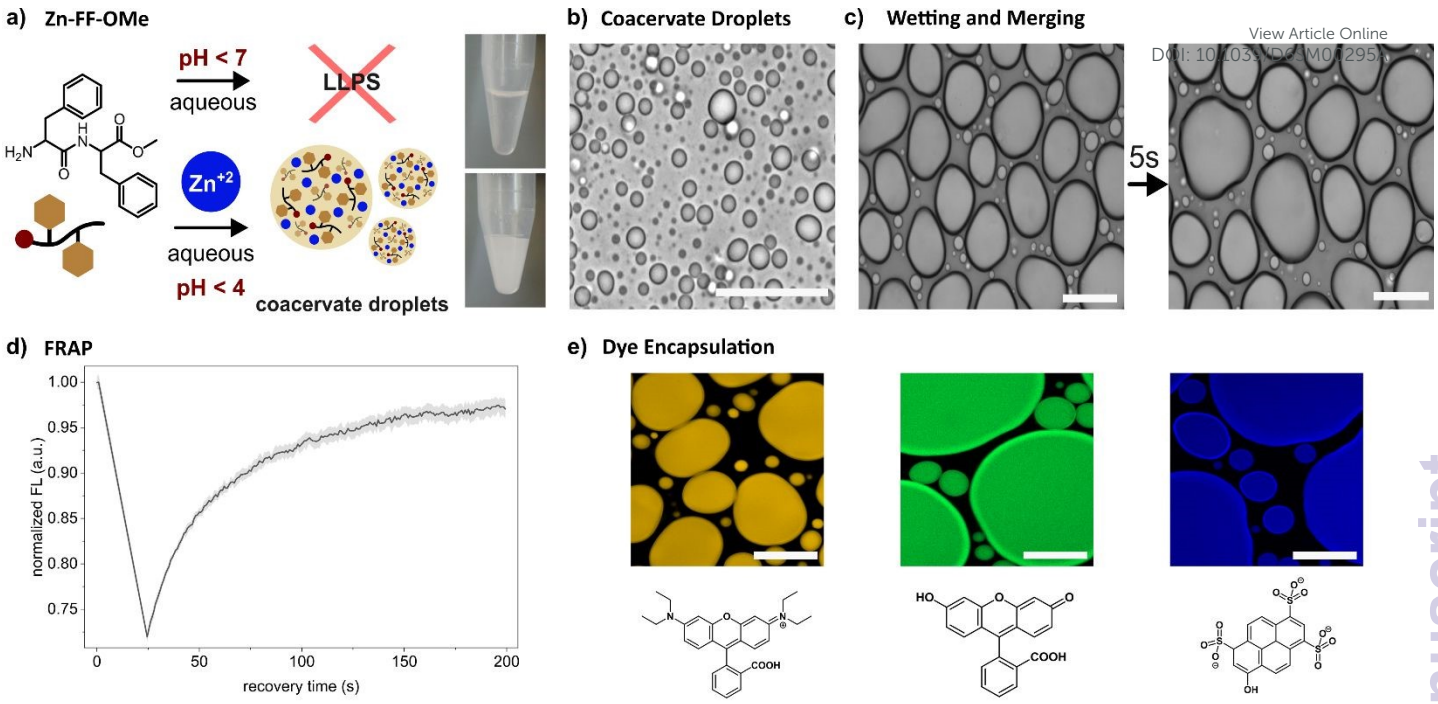

Figure 1. Formation of Zn-FF-OMe coacervates. (a) Schematic illustration of the liquid-liquid phase separation (LLPS) of FF-OMe in the presence and absence of zinc ions at acidic pH. (b) Brightfield microscopy of newly formed Zn-FF-OMe droplets. Scale bar = 20 µm. (c) Spontaneous wetting and merging of Zn-FF-OMe droplets on a microscope slide. Scale bars = 40 µm (d) Fluorescence Recovery after Photobleaching (FRAP) profile of Zn-FF-OMe coacervates. Curve represents average normalized fluorescence intensity of 5 replicate measurements with shaded area of 1 standard deviation above and below. (e) Encapsulation of rhodamine B (yellow, left), fluorescein (green, center), and pyranine (blue, right) by Zinc-FF-OMe droplets. 5 µM dye concentration. Scale bars = 20 µm. All cases: 30 mg mL^{-1} FF-OMe, 1 M $ZnCl_2$ and pH measured at 3.3-4.

spectroscopy, and microscopy indicate weak, partially hydrated Zn^{2+} interactions near the peptide carbonyl region. These interactions enrich zinc ions in the coacervate droplets, slow the liquid-solid transition, and spatially confine nucleation within droplets. Furthermore, dual-metal systems are shown to extend droplet lifetime and can be exploited as a strategy to tune internal properties such as viscosity and polarity, demonstrating that metal-mediated coacervation provides modular control over phase stability and microenvironment characteristics.

Results and Discussion

Zinc-Induced Coacervation of FF-OMe Peptide at Acidic pH

We selected L-phenylalanyl-L-phenylalanine methyl ester (FF-OMe) (**Scheme S1**) as a model peptide to investigate the effect of metal ions on the LLPS behavior of ultrashort peptides. C-terminal esterification removes the negative charge, while retaining a single protonable N-terminus, providing a simple platform to probe metal-ion-induced LLPS of charged peptides at low pH. Previous work has shown that FF-OMe undergoes coacervation under basic conditions above pH 8.[33] We hypothesized that, analogous to ion-induced aggregation in macromolecular systems, charge screening by ions could reduce electrostatic repulsion between FF-OMe molecules and promote coacervation.[34-36] Mixing 1 M $ZnCl_2$ with 30 mg mL^{-1} FF-OMe produced a highly turbid solution with a pH in the range of 3.3–4.0 (**Figure 1a**). Brightfield microscopy revealed the presence of micron-sized spherical droplets (**Figure 1b**). These droplets readily underwent fusion and surface wetting, consistent with liquid-like behavior and a low interfacial tension (**Figure 1c**). Droplet fluidity was confirmed by fluorescence recovery after photobleaching (FRAP) (**Figure 1d**). Notably, ~175 s was required to reach full recovery following only a 25% initial bleaching, indicating a highly viscous internal environment. Thermogravimetric analysis (TGA) revealed a water content of 14 wt% (**Figure S1**), consistent with a viscous and relatively hydrophobic coacervate phase.

To probe the hydrophobic character of the Zn–FF-OMe droplets, we examined their ability to partition small organic dyes. Rhodamine B, fluorescein, and pyranine were selected as aromatic probes that differ in net charge (predominantly cationic, largely neutral, and anionic, respectively) at pH 3-4 (**Figure 1e**). Zn–FF-OMe coacervates efficiently encapsulated all three dyes. Confocal microscopy indicated strong preferential localization of the dyes in the coacervate phase (**Table S1**). The weak dependence of uptake on dye charge suggests that electrostatic contributions were effectively screened under these conditions, consistent with a peptide-rich phase in which hydrophobic and π–π interactions dominate molecular partitioning. Consistent with this interpretation, FITC-labelled BSA and glucose oxidase also showed strong partitioning into the dense phase (**Figure S2**), despite acidic conditions that would typically disfavour electrostatic uptake. Together, these findings indicate that the hydrophobic Zn-FF-OMe droplet environment promotes efficient recruitment of both small molecules and larger biomacromolecules. Additionally, the coacervates enhanced a model proline-catalysed aldol reaction

View Article Online
DOI: 10.1039/D6SM00295A

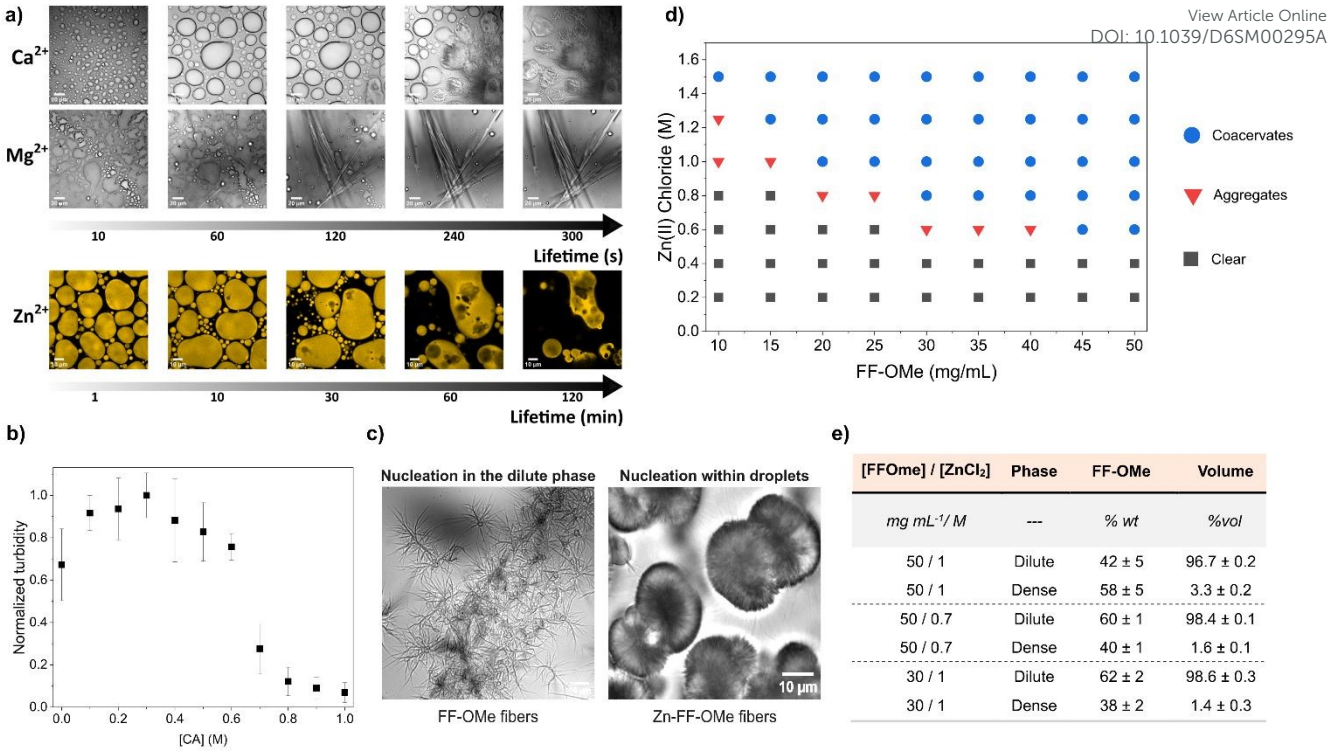

[FFOme] / [$ZnCl_2$]	Phase	FF-OMe	Volume
mg mL^{-1}/ M	---	*% wt*	*%vol*
50 / 1	Dilute	42 ± 5	96.7 ± 0.2
50 / 1	Dense	58 ± 5	3.3 ± 0.2
50 / 0.7	Dilute	60 ± 1	98.4 ± 0.1
50 / 0.7	Dense	40 ± 1	1.6 ± 0.1
30 / 1	Dilute	62 ± 2	98.6 ± 0.3
30 / 1	Dense	38 ± 2	1.4 ± 0.3

Figure 2. Composition, phase behavior and unique properties of Zn-FF-OMe coacervates. **(a)** Time evolution of FF-OMe droplets formed following the addition of $CaCl_2$, $MgCl_2$, or $ZnCl_2$, showing progression from initial liquid droplet formation to significant solidification. 30 mg mL^{-1} FF-OMe and 1 M metal chloride salt. pH 3-5. **(b)** Dissolution of the coacervate phase in the presence of zinc ion chelator citric acid. 30 mg mL^{-1} FF-OMe and 1 M $ZnCl_2$. **(c)** Brightfield images showing the liquid-to-solid transition of FF-OMe droplets prepared in the absence of Zn^{2+} under basic conditions (left) and Zn-FF-OMe droplets under acidic conditions (right). Fibers observed after complete consumption of the coacervates. 10 mg mL^{-1} FF-OMe at pH 8-9 and 30 mg mL^{-1} FF-OMe and 1 M $ZnCl_2$ at pH 3.3-4. Scale bars = 10 µm. **(d)** Dependence of FF-Ome phase separation on $ZnCl_2$ and peptide concentrations. Type of phase determined within 5 minutes of mixing via brightfield imaging and turbidity measurements. 'Aggregate' indicates gel-like particles and 'clear' indicates the lack of phase separation. **(e)** The distribution of peptide between the coacervate phase (dense) and bulk solution (dilute). %weight calculated from FF-OMe mass in each phase over total in both phases. FF-OMe concentrations quantified via absorbance (**Figure S5**) and tabulated in **Table S2**.

in water, increasing product formation by 1.5-fold as measured by NMR (**Figure S3**). Together, these results demonstrate that Zn–FF-OMe droplets function as both encapsulation compartments and reaction-enhancing microenvironments.

Effect of other metal-ions over FF-OMe coacervation and LST

We hypothesized that zinc ions promote FF-OMe coacervation via dehydration and electrostatic screening, enabling the otherwise unfavourable association of the highly soluble, positively charged peptide at acidic pH. If this mechanism is general, other metal salts should produce similar behavior. To examine the role of ionic strength in FF-OMe phase behavior, 30 mg mL^{-1} FF-OMe solutions were treated with 1 M $CaCl_2$ or $MgCl_2$ and monitored by brightfield microscopy. In both cases, micron-sized coacervate droplets formed spontaneously (**Figure 2a**), confirming that high ionic strength can induce LLPS. However, these droplets rapidly underwent a liquid-to-solid transition (LST), yielding fibrous structures within ~300 s, with initial fiber formation observed after 60-120 s. Similar behavior was observed for a broad range of other metal chloride salts (**Figure S4**). In nearly all cases, transient coacervate droplets were followed by rapid solidification within ~1–5 min. In contrast, Zn^{2+} markedly prolonged the lifetime of the coacervate phase, which persisted for up to 2 h after formation (**Figure 2a**). At this point the system was mostly composed of fibers alongside few droplets. Complete consumption of coacervates and formation of fibers was observed only after approximately 24 h. The formation of peptide fibers is consistent with the known propensity of diphenylalanine motifs to undergo π–π-driven ordered assembly, ultimately yielding tightly packed, irreversible structures.[37] These observations suggest two key features of the system. First, the ability of most metal ions to induce droplet formation indicates that dehydration and charge screening are sufficient to trigger FF-OMe coacervation at low pH. Second, because fiber formation ultimately occurs in all cases, Zn^{2+} appears to primarily modulate the kinetics of LST. Compared with other metals, Zn^{2+} substantially prolongs the lifetime of the metastable droplet phase without driving rapid LST.

To further probe the unique properties of Zn^{2+}, the metal chelator citric acid was added to pre-formed turbid suspensions containing Zn-FF-OMe coacervates. As shown in **Figure 2b**, increasing chelator concentration led to a progressive decrease in turbidity. Brightfield microscopy revealed that this trend corresponded to a reduction in droplet number and size without concomitant fiber formation (**Figure S6**), indicating dissociation of the coacervate phase rather than conversion via LST. These results support a model in which Zn^{2+} directly stabilizes the droplet phase. Notably, a modest turbidity increase observed at ≤0.2 M citric acid is attributed to partial

View Article Online
DOI: 10.1039/D5SM02951

dehydration effects of the additive and/or partition into the droplets.

Time-resolved brightfield microscopy was used to follow the evolution of freshly prepared Zn-FF-OMe suspensions. Within 5 minutes, droplets sedimented and merged at the substrate surface. After 15 minutes, LST initiated within individual droplets. Needle-like structures nucleated internally and slowly expanded, with liquid and solid phases coexisting for up to 2 hours (**Figure S7**). Even after complete LST, fibrous structures remained confined within the original droplet volume. In contrast, under basic conditions, fiber nucleation occurred throughout the bulk solution **(Figure 2c)**, with fibrous networks propagating across droplets rather than emerging from within them. This difference indicates that zinc-induced coacervation follows a distinct transformation pathway in which nucleation is spatially confined to the droplet interior. Together, these results show that Zn^{2+} not only initiates LLPS at acidic pH but also modulates the kinetics and spatial pathway of subsequent solidification.

Effect of Zn-FF-OMe Coacervate Composition on Phase Transitions

To understand how composition governs coacervation, we systematically varied the concentrations of $ZnCl_2$ and FF-OMe and constructed a phase diagram based on turbidity measurements and brightfield microscopy (**Figure 2d**). Increasing the peptide concentration lowered the amount of $ZnCl_2$ required to induce LLPS. No droplet formation was observed below 0.6 M $ZnCl_2$ or 10 mg mL^{-1} FF-OMe, indicating threshold concentrations for both components. Between the homogeneous region and the LLPS region, ill-defined and gel-like aggregates were detected, suggesting that insufficient zinc promotes gelation rather than droplet formation. This intermediate regime became less pronounced under peptide-rich conditions. Overall, coacervation occurred within a defined compositional window.

We then quantified how peptide distributes between the dense and dilute phases. Immediately after droplet formation, the two phases were separated, their volumes measured, and peptide concentrations determined by absorbance spectroscopy (**Figure 2e**). In a system containing 50 mg mL^{-1} FF-OMe and 1 M $ZnCl_2$, the dense phase accounted for 3.3% of the total solution volume but contained ~60% of the total peptide mass. Reducing either $ZnCl_2$ by 30% or FF-OMe by 40% resulted in a dense phase occupying 1.6% and 1.4% of the total volume, respectively. In addition, the fraction of peptide in the dense phase decreased by approximately 20% compared to the 50:1 reference composition. These results show that both droplet yield and peptide enrichment scale with the overall peptide: Zn^{2+} ratio. Although high concentrations of both components are required to induce LLPS, only a portion of the total peptide partitions into the coacervate phase, with a significant fraction remaining in solution.

Lastly, we examined how Zn^{2+} partitions between the dense and dilute phases before and after the liquid–solid transition. Freshly prepared suspensions were separated into coacervate and bulk phases, while a control sample was allowed to fully undergo LST before the resulting fibers were removed from solution. Zinc concentrations were determined via flame atomic absorption spectroscopy (FAAS) (**Figure S8**). Prior to LST, Zn^{2+} is enriched in the dense phase by a factor of ~1.8 relative to the bulk solution, whereas the coacervate phase contained peptide and zinc ions in an approximate 5:4 ratio **(Table S3)**. This comparable abundance indicates substantial peptide-zinc association within the droplets. After complete LST and removal of fibers, the Zn^{2+} concentration in the supernatant returned to its initial value. This indicates that zinc ions are released during solidification and is not incorporated into the final solid fibrous material. Powder X-ray diffraction confirmed that the fibers exhibited the same diffraction pattern as pure FF-OMe (**Figure S9**), consistent with peptide-only fibers. Together, these results show that zinc ions kinetically stabilize the droplet dense phase, while slow zinc release accompanies the transition to the thermodynamically favoured peptide fiber.

Zinc-Peptide Interactions Behind Coacervate Stabilization and Liquid-to-Solid Transition

Coordination of Zn^{2+} to electron-rich groups in FF-OMe would be expected to perturb local bond environments and induce shifts in vibrational frequencies. To examine this, we compared the infrared spectra of Zn-FF-OMe coacervates (pH 3.3-4) with FF-OMe coacervates (pH 9) in the absence of zinc ions and fully dissolved FF-OMe (pH 5) (**Figure 3**). This comparison isolates spectral changes associated with the presence of zinc ions. The main differences between the two coacervate systems were observed in bands a and b, assigned to the methyl ester and amide I carbonyl stretches, respectively. In both cases, only minor shifts (≤10 cm^{-1}) were detected with the most significant being the amide I band. These small but reproducible changes suggest interaction of Zn^{2+} in the carbonyl region of the peptide. The limited magnitude of the observed shifts indicates that any zinc-peptide interaction is weak, as stronger carbonyl chelation typically produces larger vibrational changes.[38-40] This interpretation is consistent with our earlier finding that Zn^{2+} is absent from the final fibers, indicating that zinc ions are neither strongly nor permanently incorporated during solidification.

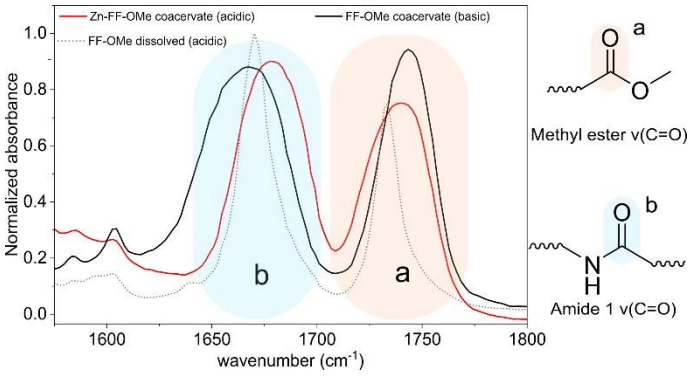

Figure 3. Effect of Zn^{+2} on FF-OMe FT-IR Spectra. Spectra of FF-OMe solution and two coacervate phases prepared under acidic (Zn-FF-OMe coa.) or basic conditions (FF-OMe coa.). 30 mg mL^{-1} FF-OMe at pH 8-9 and 50 mg mL^{-1} FF-OMe and 1 M $ZnCl_2$ at pH 3.3-4.

View Article Online
DOI: 10.1039/D6SM00295A

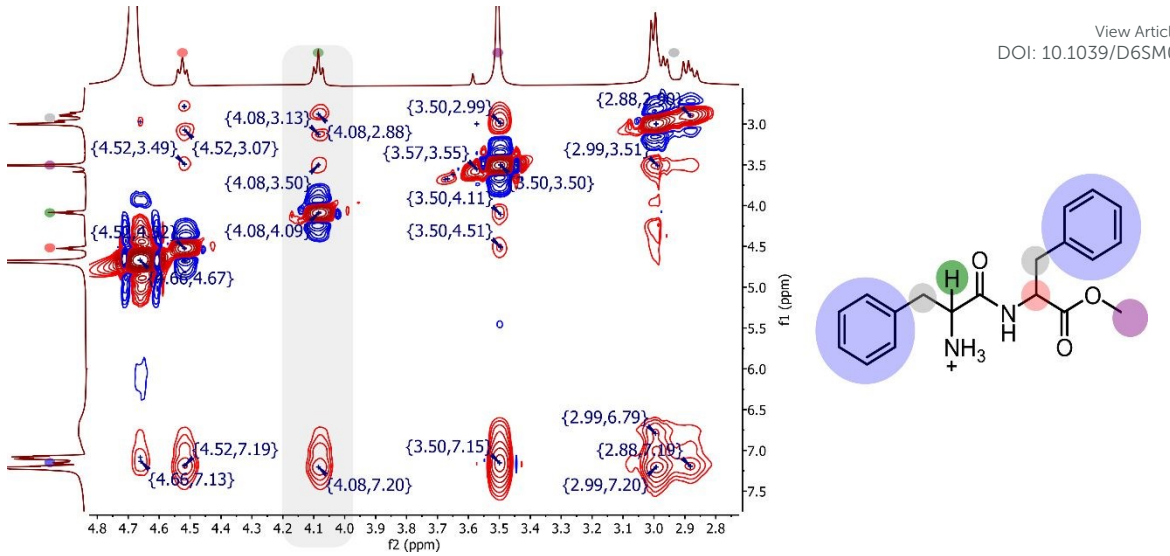

Figure 4. 2D-HNMR (NOESY) spectrum. Focus on the aliphatic region of a freshly prepared coacervate suspension. Shaded area highlights the unique set of peaks found only in the Zinc-FF-OMe system between amide adjacent proton (green) and all other peptide signals. 1M $ZnCl_2$ and 30 mg mL^{-1} FF-OMe in D_2O.

To further assess how zinc affects molecular organization within the coacervate, we employed two-dimensional ^1H NOESY NMR spectroscopy, which probes through-space proximity between nuclei. The NOESY spectra of both basic FF-OMe and Zn-FF-OMe coacervates feature a broad aromatic signal at 6.75 ppm associated with the condensed phase (**Figures 4, S10**). In contrast, the Zn–FF-OMe coacervate displays additional correlation signals involving the amide-adjacent proton (~4.1 ppm) and multiple peptide protons. These correlations were absent in the basic FF-OMe coacervate sample, which did not contain zinc ions, and in the absence of coacervates in a Zn^{2+} and FF-OMe solution below the critical coacervation concentration (**Figure S11**). This suggests that the presence of Zn^{2+} alters intermolecular packing or local peptide organization when peptide concentration is close to the critical value. DLPNO-CCSD(T)-LED calculations indicate that Zn^{2+} binds the peptide via coordination to carbonyl oxygens (**Figure S12**), but that complex formation is energetically disfavoured in aqueous solution (**Table S4**). This is consistent with the small FTIR shifts observed (**Figure 3**), indicating weak Zn^{2+}-carbonyl interactions. Nevertheless, such interactions may contribute to coacervate formation, where release of structured water provide favourable entropic stabilization not captured in the present model.

We then investigated the mechanism of the liquid–to-solid transition. Because fiber formation initiates within droplets, we monitored the dense phase before and during LST using confocal microscopy coupled with Raman spectroscopy. Confocal imaging revealed an initially homogeneous coacervate phase, followed by the appearance of dark regions and subsequently growing fibrous structures (**Figure S13**). Rhodamine B was used to visualize the peptide-rich phase. Raman spectra confirmed that both the dense phase and the growing fibers exhibited characteristic FF-OMe peaks at 1003 (a), 1030 (b), 1205 (c), and 1585-1605 cm^{-1} (d) (**Figure 5**).[41] The dark regions display dominant water signals, particularly at ~3500 cm^{-1} (e), indicating localized water enrichment within the coacervate phase prior to fiber formation. These observations suggest that expulsion of water from the dense phase occurs during the transition from liquid-like coacervate to solid fibers. Given the weak zinc-peptide interactions, it is likely that zinc ions are released as the peptide phase dehydrates and reorganizes into solid fibers. Thus, zinc ions appear to stabilize the hydrated dense phase, while its release accompanies the progression toward the thermodynamically favoured solid phase. Raman confocal spectroscopy shows that the Zn^{2+}-rich coacervate phase has a distinct but low intensity OH-stretching profile, with sharp features near ~3200 cm^{-1} rather than the broad shoulder typically associated with ordered water (**Figure S14**). This suggests a shift in hydration environment within the coacervate phase.[42, 43]

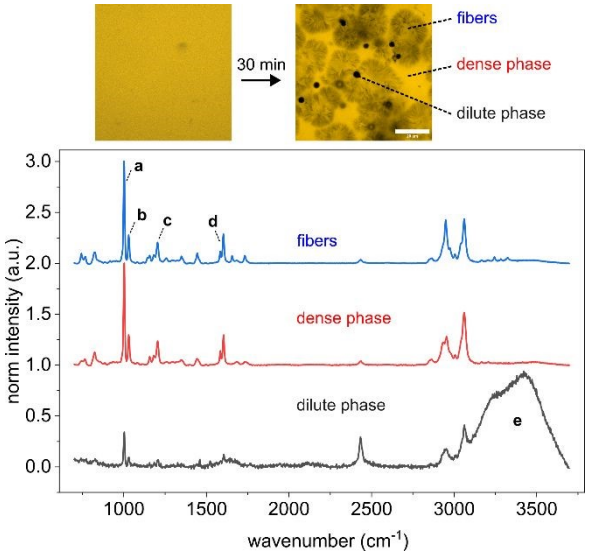

Figure 5. Raman spectra of the different phases observed during the liquid-to-solid transition of Zn-FF-OMe. 1M $ZnCl_2$ and 50 mg mL^{-1} FF-OMe.

View Article Online
DOI: 10.1039/D6SM00295A

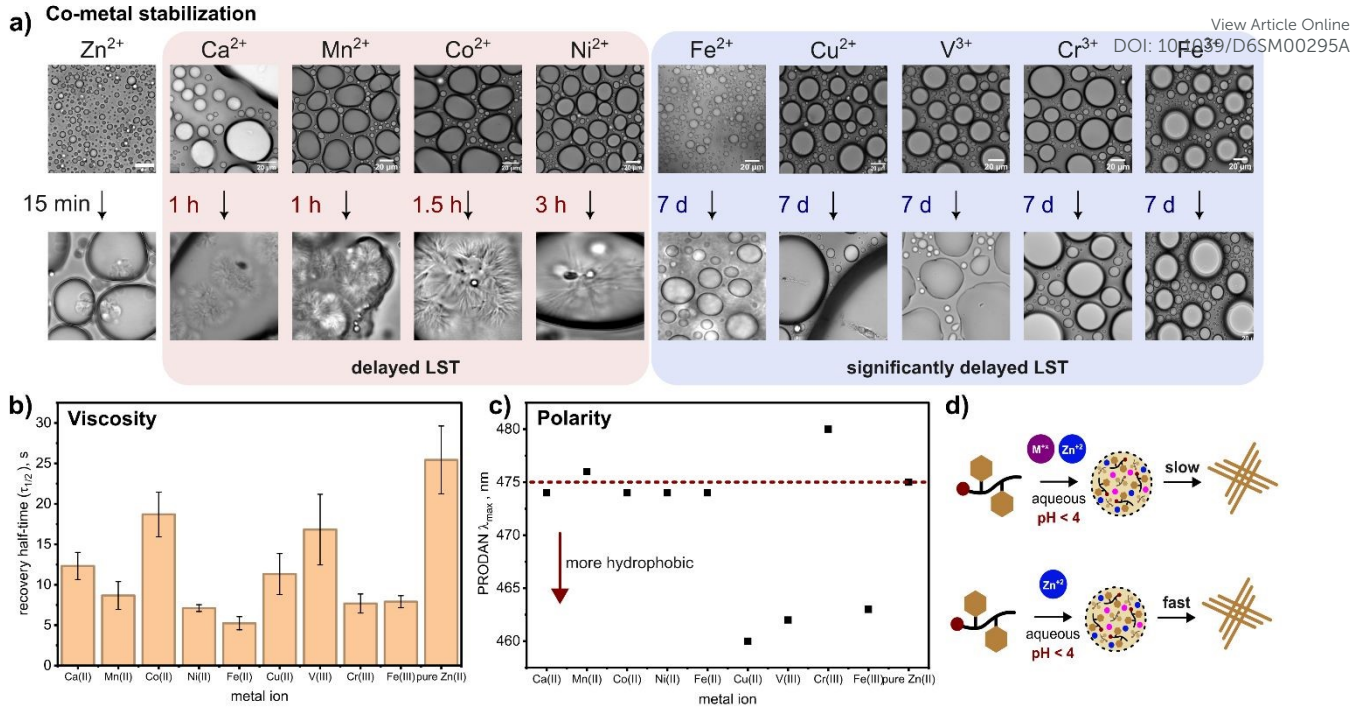

Figure 6. Co-Metalation induced stability and variability in Zn-FF-Ome coacervates. (a) The capacity of various metals chloride salts at inhibiting Zn-FF-Ome LST. Brightfield images display the coacervate systems right after preparation and either right after the observation of LST or after 7 days in its absence. LST onset refers to time of LST initiation. (b, c) The effects of secondary metals on the physical and chemical properties of Zinc-FF-OMe coacervates in terms of microenvironment (b) viscosity and (c) polarity. Average recovery half-life of rhodamine B over 5 replicate measurements. PRODAN excited at 360 nm. (d) Schematic illustration of proposed secondary metal incorporation in Zn-FF-OMe coacervates for enhanced stability. All cases: 30 mg mL^{-1} FF-Ome, 1 M $ZnCl_2$ and 0.5 M of the specified metal chloride salt

Proposed Mechanism for Zinc-Mediated FF-OMe Coacervation

Based on our observations, we propose the following mechanism for zinc-mediated coacervation. At high ionic strength, water activity decreases and repulsion between protonated peptides is reduced, enabling peptide association and droplet formation. In parallel, Zn^{2+} engages in interactions near the amide carbonyl region of the peptide. These interactions are not strongly favourable in solution but become more prominent at high peptide and salt concentrations. Within the coacervate phase, zinc ions are enriched and remain partially hydrated. Rather than forming strong chelates, Zn^{2+} appears to act as a transient bridge between peptide molecules while retaining coordinated water. This weak and reversible association stabilizes a hydrated, peptide-rich liquid state. Over time, local rearrangements within the crowded coacervate allow π–π interactions between diphenylalanine motifs to dominate. Nucleation eventually occurs inside the droplets, and peptide stacking progressively excludes water. As the system dehydrates and reorganizes into solid fibrous structure, Zn^{2+} is released back into solution. The growing fibers eventually consume the dense phase, restoring zinc ions and water to the bulk. This role of Zn^{2+} as a modulator of assembly is consistent with related metal-mediated systems in aqueous media.[44-46]

Dual-metal System Inhibits LST and Introduces Modularity

Although our results show that Zn^{2+} delays liquid to solid transition, it does not fully prevent it. However, we observed that the presence of secondary metal ions further stabilized the droplets against fiber formation (**Figure 6**). The extent of the stabilization depended on the metal ion identity. To test this, nine identical dispersions of 30 mg mL^{-1} and 1 M $ZnCl_2$ were prepared, each doped with 0.5 M of a different metal chloride salt. Samples were monitored to detect the first instance of LST over a 7-day period **(Figure 6a)**. In the case of a pure Zn-FF-OMe system, LST onset took place only after 15 minutes of droplet formation. In all other cases, the presence of a co-metal either delayed LST onset by at least 1 hour or prevented it completely during the 7-day observation period. Importantly, $ZnCl_2$ had to be added first or simultaneously. When other metal salts were added prior to zinc ions, rapid and irreversible LST occurred. The degree of stabilization varied as a function of metal identity and likely reflects differences in charge density, ionic radius, and hydration strength. Phase diagrams constructed as a function of zinc and co-metal concentration (**Figure S15**) show distinct shifts in phase boundaries, supporting direct involvement of the added metal ions in modulating the Zn-FF-OMe system. Notably, coacervation could be achieved at lower $ZnCl_2$ concentrations when a co-metal was present, consistent with zinc ions primarily stabilizing the droplets while dehydration and additional charge screening can be achieved by additional salts. The effect of composition on the liquid-to-solid transition (LST) was examined using Zn–FF-OMe coacervates with increasing $CaCl_2$ (**Figure S16**). Higher co-metal concentrations led to greater droplet persistence at 1 h. After 24 h, only the 1 M sample retained significant droplets, indicating that fiber formation decreases with co-metal content. These results show that co-metals slow coacervate solidification in a concentration-dependent manner. Then, we examined how mixed-metal systems influenced droplet properties (**Figure 6b**). Co-metal

addition altered pH, droplet viscosity, and microenvironment polarity. Owing to their Lewis acidity, co-metal salts enabled droplet stabilization at lower pH values **(Table S5).** In addition, the presence of a co-metal reduced droplet viscosity, consistent with either increased water retention or weakened peptide–peptide interactions (**Table S6)**. Despite these changes, the coacervate phase remained hydrophobic. PRODAN, a polarity-sensitive probe, indicated that Zn–FF-OMe droplets had a polarity between acetonitrile and ethanol (**Figure S17**).[47] Doping with Cu^{2+} shifted the emission toward acetonitrile-like polarity, whereas Cr^{3+} shifted it toward ethanol-like polarity. These changes indicate that secondary metals directly influence the internal environment of the droplets and further support their role in modulating coacervate stability.

Finally, we investigated the mechanism by which secondary metals enhance Zn-FF-OMe droplet stability. FAAS measurements indicate that Zn^{2+} remains ~2-fold enriched within the coacervate phase even in the presence of Fe^{3+}, while Fe^{3+} preferentially partitions into the dilute phase (**Figures S18–S19**). TGA (**Figure S20**) and FT-IR data (**Figure S21**) show only minor changes in hydration (13–15 wt%) and peptide intermolecular interactions upon co-metal addition, whereas 2D NOESY with Ca^{2+} (**Figure S22**) suggests a less tightly packed peptide arrangement. Together, these results suggest that secondary metals may stabilize Zn-FF-OMe coacervates through subtle perturbations in peptide packing and possibly hydration within the coacervate phase.

Conclusions

In summary, we reported a zinc-mediated route to induce liquid-liquid phase separation of a minimal diphenylalanine peptide under acidic conditions. Zn^{+2} enrichment within the dense phase and partially hydrated interactions near the amide carbonyl stabilize a metastable liquid state prior to an irreversible liquid-solid transition into peptide fibers. Water redistribution accompanies solidification, with zinc released back into solution, highlighting its role as a modulator rather than a structural component of the final solid material. Introduction of secondary metal ions further extends droplet lifetime by inhibiting fiber formation and tunes internal properties, demonstrating that metal-peptide interactions can regulate phase behavior and assembly pathways in minimal peptide systems. This work is relevant to the engineering of dynamic soft materials whose properties can be modulated by the presence of metal ions. Short peptides are also considered plausible building blocks in prebiotic environments. The ability of metal ions to induce condensate formation from minimal peptides suggests a potential mechanism by which coacervate-like compartments could have been regulated prior to the emergence of membrane-bound protocells. Consistent with this idea, the catalytically active tripeptide PFF-OMe also formed micron-sized coacervate droplets upon $ZnCl_2$ addition (**Figure S23**),[48] indicating that this behavior may be a general feature of short aromatic peptides. While preliminary, these results provide a basis for further optimization of Zn–FF-OMe coacervates as encapsulation platforms and aqueous reaction media. Future efforts will focus on reducing metal loadings, improving control over pH and microenvironment properties, and eliminating LST.

Author contributions

M.A.B.: investigation, formal analysis, methodology, writing. M.R., L.G., O.Y., G.Z.: investigation. L.C.S.: conceptualization, methodology, writing, resources.

Conflicts of interest

There are no conflicts to declare.

Acknowledgements

We acknowledge support from the Natural Sciences and Engineering Research Council of Canada (NSERC; Discovery Grant, RGPIN-2024-04752), the Centre en Chimie Verte et Catalyse (CCVC), and the Canada Foundation for Innovation (CFI; Project No. 45056).

Notes and references

1. M. Marguet, C. Bonduelle and S. Lecommandoux, *Chemical Society Reviews*, 2013, **42**, 512-529.
2. B. S. Glick and A. Nakano, *Annual Review of Cell and Developmental Biology*, 2009, **25**, 113-132.
3. L. Bar-Peled and N. Kory, *Nature Metabolism*, 2022, **4**, 1232-1244.
4. C. P. Brangwynne, C. R. Eckmann, D. S. Courson, A. Rybarska, C. Hoege, J. Gharakhani, F. Jülicher and A. A. Hyman, *Science*, 2009, **324**, 1729-1732.
5. I. A. Sawyer, D. Sturgill and M. Dundr, *WIREs RNA*, 2019, **10**, e1514.
6. Y. Liu, Y. Li and P. Zhang, *Protein Cell*, 2025, **16**, 418-438.
7. F.-J. Ruiz, S. Rubio and D. Pérez-Bendito, *Analytical Chemistry*, 2007, **79**, 7473-7484.
8. T. Beneyton, C. Love, M. Girault, T.-Y. D. Tang and J.-C. Baret, *ChemSystemsChem*, 2020, **2**, e2000022.
9. L. Zhou, H. Shi, Z. Li and C. He, *Macromolecular Rapid Communications*, 2020, **41**, 2000149.
10. E. A. Frankel, P. C. Bevilacqua and C. D. Keating, *Langmuir*, 2016, **32**, 2041-2049.
11. N. A. Yewdall, A. A. M. André, T. Lu and E. Spruijt, *Current Opinion in Colloid & Interface Science*, 2021, **52**, 101416.
12. R. Harris, N. Berman and A. Lampel, *Chemical Society Reviews*, 2025, **54**, 4183-4199.
13. S. L. Higashi and M. Ikeda, *Advanced Biology*, 2025, **9**, 2400572.
14. S. P. Moulik, A. K. Rakshit, A. Pan and B. Naskar, *Colloids and Interfaces*, 2022, **6**, 45.
15. F. Pir Cakmak, A. M. Marianelli and C. D. Keating, *Langmuir*, 2021, **37**, 10366-10375.

16. H. M. Fares, Y. E. Ghoussoub, J. D. Delgado, J. Fu, V. S. Urban and J. B. Schlenoff, *Macromolecules*, 2018, **51**, 4945-4955.
17. E. Spruijt, A. H. Westphal, J. W. Borst, M. A. Cohen Stuart and J. van der Gucht, *Macromolecules*, 2010, **43**, 6476-6484.
18. D. Priftis and M. Tirrell, *Soft Matter*, 2012, **8**, 9396-9405.
19. C. Yuan, R. Xing, J. Cui, W. Fan, J. Li and X. Yan, *CCS Chemistry*, 2024, **6**, 255-265.
20. J. Yuan, Y. Yang, K. Dai, R. Fakhrullin, H. Li, P. Zhou, C. Yuan and X. Yan, *ACS Applied Materials & Interfaces*, 2025, **17**, 27697-27712.
21. F. Sheehan, D. Sementa, A. Jain, M. Kumar, M. Tayarani-Najjaran, D. Kroiss and R. V. Ulijn, *Chemical Reviews*, 2021, **121**, 13869-13914.
22. Y. Tang, S. Bera, Y. Yao, J. Zeng, Z. Lao, X. Dong, E. Gazit and G. Wei, *Cell Reports Physical Science*, 2021, **2**.
23. X. Wu, Y. Sun, J. Yu and A. Miserez, *Communications Chemistry*, 2024, **7**, 5.
24. A. Shebanova, Q. M. Perrin, K. Zhu, S. Gudlur, Z. Chen, Y. Sun, C. Huang, Z. W. Lim, E. A. Mondarte, R. Sun, S. Lim, J. Yu, Y. Miao, A. N. Parikh, A. Ludwig and A. Miserez, *Advanced Science*, 2024, **11**, 2402652.
25. S. Cao, P. Zhou, G. Shen, T. Ivanov, X. Yan, K. Landfester and L. Caire da Silva, *Nature Communications*, 2025, **16**, 2407.
26. M. Abbas, W. P. Lipiński, K. K. Nakashima, W. T. S. Huck and E. Spruijt, *Nature Chemistry*, 2021, **13**, 1046-1054.
27. Y. Zhang, R. Prasad, S. Su, D. Lee and H.-X. Zhou, *Cell Reports Physical Science*, 2024, **5**, 102218.
28. C. Firdharini, I. Yildiz, H. AlNaqbi and M. Abbas, *ChemSystemsChem*, 2025, **7**, e00027.
29. X. Li, T. Zheng, X. Liu, Z. Du, X. Xie, B. Li, L. Wu and W. Li, *Langmuir*, 2019, **35**, 4995-5003.
30. Y. Huang, J. Huang, W. Yin, F. Xie, B. Coleman, Y. Cao, S. Aya, W. Zhu, Z. Yang and L. Jiang, *ACS Nano*, 2023, **17**, 6234-6246.
31. P. L. Onuchic, A. N. Milin, I. Alshareedah, A. A. Deniz and P. R. Banerjee, *Scientific Reports*, 2019, **9**, 12161.
32. X. Liu, Z. Ma, J. Nie, J. Fang and W. Li, *Biomacromolecules*, 2022, **23**, 1009-1019.
33. S. Cao, T. Ivanov, J. Heuer, C. T. J. Ferguson, K. Landfester and L. Caire da Silva, *Nature Communications*, 2024, **15**, 39.
34. W. Wang, Y. Xu, A. Li, T. Li, M. Liu, R. von Klitzing, C. K. Ober, A. B. Kayitmazer, L. Li and X. Guo, *RSC Advances*, 2015, **5**, 66871-66878.
35. M. Ramesh, C. Balachandra, P. Baruah and T. Govindaraju, *Journal of Peptide Science*, 2023, **29**, e3465.
36. J. B. Rayman, K. A. Karl and E. R. Kandel, *Cell Rep*, 2018, **22**, 59-71.
37. C. Yuan, A. Levin, W. Chen, R. Xing, Q. Zou, T. W. Herling, P. K. Challa, T. P. J. Knowles and X. Yan, *Angewandte Chemie International Edition*, 2019, **58**, 18116-18123.
38. H. A. Tajmir-Riahi and A. Ahmed, *Journal of Molecular Structure*, 1993, **297**, 103-108.
39. S. Nahar and H. A. Tajmir-Riahi, *Journal of Colloid and Interface Science*, 1996, **178**, 648-656.
40. T. Dudev and C. Lim, *Journal of Molecular Structure*, 2012, **1009**, 83-88.
41. B. Hernández, F. Pflüger, S. G. Kruglik and M. Ghomi, *Journal of Raman Spectroscopy*, 2013, **44**, 827-833.
42. M. J. Taylor and E. Whalley, *The Journal of Chemical Physics*, 1964, **40**, 1660-1664.
43. H. Suzuki, Y. Matsuzaki, A. Muraoka and M. Tachikawa, *The Journal of Chemical Physics*, 2012, **136**.
44. H.-X. Zhou, *Proteins: Structure, Function, and Bioinformatics*, 2005, **61**, 69-78.
45. Y. Liu, B. Momani, H. H. Winter and S. L. Perry, *Soft Matter*, 2017, **13**, 7332-7340.
46. V. Vaissier Welborn, W. R. Archer and M. D. Schulz, *Journal of Chemical Information and Modeling*, 2023, **63**, 2030-2036.
47. O. A. Kucherak, P. Didier, Y. Mély and A. S. Klymchenko, *The Journal of Physical Chemistry Letters*, 2010, **1**, 616-620.
48. Z. Dai, M. Meyn and L. Caire da Silva, *Chemical Communications*, 2026, **62**, 2264-2267.

View Article Online
DOI: 10.1039/D6SM00295A

All data supporting the findings of this study are available in the article, its supplementary information, and the associated source data files, which have been deposited in the McGill University Dataverse (https://doi.org/10.5683/SP3/1SYG8Y) and are publicly accessible under a CC BY 4.0 license.

***Note to the editor**: The dataset associated with this manuscript has been deposited in the McGill University Dataverse and will be made publicly accessible upon publication under the same DOI referenced above. During the peer review process, a private access link can be provided upon request.*